Mon. Not. R. Astron. Soc. **000**, 000–000 (0000) Printed 10 October 2016 (MN LATEX style file v2.2)

Diagnosing galactic feedback with line broadening in the low redshift Lyman-α forest

Matteo Viel[1,2⋆], Martin G. Haehnelt[3] , James S. Bolton[4], Tae-Sun Kim[1], Ewald Puchwein[3], Fahad Nasir[4] & Bart P. Wakker[5]
[1] *INAF - Osservatorio Astronomico di Trieste, Via G.B. Tiepolo 11, I-34131 Trieste, Italy*
[2] *INFN/National Institute for Nuclear Physics, Via Valerio 2, I-34127 Trieste, Italy*
[3] *Kavli Institute for Cosmology and Institute of Astronomy, Madingley Road, Cambridge, CB3 0HA, UK*
[4] *School of Physics and Astronomy, University of Nottingham, University Park, Nottingham, NG7 2RD, UK*
[5] *Supported by NASA/NSF, affiliated with Dept. of Astronomy, University of Wisconsin-Madison, 475 N. Charter Street, Madison, WI 53706, USA*

arXiv:1610.02046v1 [astro-ph.GA] 6 Oct 2016

10 October 2016

ABSTRACT

We compare the low redshift ($z \simeq 0.1$) Ly-α forest from hydrodynamical simulations with data from the Cosmic Origin Spectrograph (COS). We find tension between the observed number of lines with b-parameters in the range 25–45 km s^{-1} and the predictions from simulations that incorporate either vigorous feedback from active galactic nuclei or that exclude feedback altogether. The gas in these simulations is, respectively, either too hot to contribute to the Ly-α absorption or too cold to produce the required line widths. Matching the observed $b-$parameter distribution therefore requires feedback processes that thermally or turbulently broaden the absorption features without collisionally (over-)ionising hydrogen. This suggests the Ly-α forest b-parameter distribution is a valulable diagnostic of galactic feedback in the low redshift Universe. We furthermore confirm the low redshift Ly-α forest column density distribution is better reproduced by an ultraviolet background with an H I photo-ionisation rate a factor 1.5–3 higher than predicted by Haardt & Madau (2012).

Key words: cosmology: diffuse radiation – large-scale structure of Universe – methods: numerical – galaxies: intergalactic medium – quasars: absorption lines

1 INTRODUCTION

Ly-α forest data have become an important tool in studying the physical state of the intermediate redshift ($2 < z < 5$) intergalactic (IGM) and circumgalactic medium. With the advent of the Cosmic Origins Spectrograph (COS) on the *Hubble Space Telescope (HST)*, it has become possible to obtain much improved measurements also at lower redshift (Savage et al. 2014; Shull et al. 2014; Danforth et al. 2016; Werk et al. 2016; Pachat et al. 2016). The increased resolution and signal-to-noise (S/N) of the COS data enables the measurement of the column density of Ly-α absorbers to lower values and helps resolve the thermal broadening for weaker absorbers, complementing earlier investigations of the low-redshift IGM (Weymann et al. 1998; Janknecht et al. 2006; Kirkman et al. 2007).

Concurrently, the interpretation of these data has been aided by high dynamic range cosmological hydrodynamical simulations incorporating much of the relevant (subgrid) physics at $z = 0$ (Tornatore et al. 2010; Davé et al. 2010; Ford et al. 2013; Villaescusa-Navarro et al. 2016; Rahmati et al. 2016). The present consensus on the nature of these absorbers is that they trace galactic environments relatively faithfully and may be used to address a wide set of scientific questions, from finding the missing baryons to the nature of the ultraviolet background (UVB) and galactic feedback. Here, we compare a new measurement of the observed H I Ly-α Doppler b-parameter and column density distribution at $z = 0.1$ with predictions from a range of state-of-the-art numerical simulations. We assess whether constraints on the physical mechanism responsible for stellar and active galactic nuclei (AGN) feedback may be obtained, and revisit the possible missing ionising photon problem first discussed by Kollmeier et al. (2014) and further investigated by Shull et al. (2015), Wakker et al. (2015), Khaire & Srianand (2015) and Gurvich et al. (2016).

2 COS DATA

We have selected 44 *HST*/COS AGN spectra available as of December 2015 in the *HST* MAST (Mikulski Archive for

⋆ email: viel@oats.inaf.it

© 0000 RAS

Space Telescopes). The two main selection criteria are: a S/N per resolution element that is larger than 20 and an emission redshift in the redshift range $0.1 < z < 0.35$, covering the Ly-α forest at $0 < z < 0.2$. The first criterion was imposed so that the detection limit is $\log N_{\rm H\,I}/{\rm cm}^{-2} \sim 13$. The final co-added COS spectra have a resolution of ~ 18–20 km s^{-1} in a heliocentric velocity frame and have S/N $\in [30-150]$ per resolution element in the Ly-α forest region. The total redshift coverage is $\Delta z = 4.991$ excluding Milky Way interstellar medium line contamination and unobserved wavelength regions. Details of the COS data reduction and the properties of the AGN spectra can be found in Wakker et al. (2015) and Kim et al. (2016, *in prep.*), respectively.

After initial continuum fitting, all the absorption profiles were identified and fitted with a Voigt profile using `VPFIT` (Carswell & Webb 2014) to obtain the column density and the $b-$parameter (see Kim et al. 2013, 2016, for more details). `VPFIT` is also used to obtain line parameters for our simulated spectra. Since the simulated spectra are fitted only with H I Ly-α lines, we have also fitted the observed Ly-α lines without using any higher-order Lyman series lines. Depending on the date of the observation, a non-Gaussian COS line spread function (LSF) at the different lifetime position was used (Kriss 2011). At $0 < z < 0.2$, the total number of fitted H I lines is 704 at $\log N_{\rm H\,I}/{\rm cm}^{-2} \in [12.5, 14.5]$, with the b-parameters spanning the range 8–181 km s^{-1}. There are 424 lines with $\log N_{\rm H\,I}/{\rm cm}^{-2} \in [13, 14]$ with a relative error on the b-parameter smaller than 0.5: this will constitute our main sample. For comparison, we shall also use the Ly-α lines obtained by Danforth et al. (2016) from 39 COS AGN ($\Delta z = 4.33$). We find good agreement between the data set used here and the one presented in Danforth et al. (2016) (D16), as will be demonstrated later.

3 NUMERICAL SIMULATIONS

We consider a range of state-of-the art ΛCDM cosmological hydrodynamic simulations including the Illustris (Vogelsberger et al. 2014) and Sherwood (Bolton et al. 2016) simulations. The majority of the simulations have been performed with the parallel Tree-PM smoothed particle hydrodynamics (SPH) code P-Gadget-3 (Springel 2005), apart from Illustris that was run with the moving-mesh code AREPO (Springel 2010). The simulations include a variety of star formation and stellar or AGN feedback implementations as well as a range of UVB models. We have also boosted the He II photo-heating rates in some models in an ad hoc manner (as described in Bolton et al. 2008) to obtain temperatures for the low density, photo-ionised IGM that better match the observed b-parameter distribution. The main properties of the individual simulations are as follows.

HM (Haardt & Madau UVB models). These are P-Gadget-3 simulations with a range of assumptions for the UVB and temperature of the low density IGM. HM simulations are performed without feedback using a simplified star formation criterion that turns all gas particles with a density above $\rho/\langle\rho\rangle = 10^3$ and a temperature below 10^5 K into star particles. This feature is labelled `QUICKLYA` and was first used by Viel et al. (2004). The HM01 runs (Haardt & Madau 2001) differ from the HM12 simulations (Haardt & Madau 2012) in the choice of precomputed UVB model and hence H I photo-ionisation rate. In addition, the thermal history for each simulation is labelled as "hot" or "vhot", indicating a different assumption for the gas temperature, T_0, at the mean background density. All the HM models are run with a linear box size of $60h^{-1}$ comoving Mpc and 2×512^3 gas and dark matter particles.

Illustris. The Illustris simulation has a linear box size of $75h^{-1}$ comoving Mpc and follows the evolution of 2×1820^3 gas cells and dark matter particles. The star formation and feedback model uses supernovae-driven winds which scale with the velocity dispersion of the host halo (Vogelsberger et al. 2013). AGN feedback is based on Sijacki et al. (2007) and uses two models – radiatively efficient and "radio-mode" – depending on the black hole accretion rate. In the latter case 7 per cent of the accreted rest mass energy is thermally injected into AGN bubbles. The individual injection events are highly energetic, corresponding to roughly $0.01 M_{\rm BH} c^2$. Photo-ionisation and heating is followed using the Faucher-Giguère et al. (2009) UVB, and self-shielding and ionising flux from nearby AGN is accounted for.

Sherwood. The Sherwood simulation that we primarily use here was performed with a linear box size of $80h^{-1}$ comoving Mpc and 2×512^3 particles. It employs the star formation and feedback model described in Puchwein & Springel (2013). This follows the star formation prescription of Springel & Hernquist (2003) with a Chabrier initial mass function and supernovae driven winds with velocities that scale with the escape velocity of the galaxy. The AGN feedback is again based on Sijacki et al. (2007), but with more modest assumptions about the available energy; 2 per cent of the accreted rest mass energy is injected in the radio mode and individual events are much less energetic, with $\gtrsim 2 \times 10^{-6} M_{\rm BH} c^2$. In addition two further Sherwood runs at different resolution are used for convergence testing (not show in any of the figures). These use the simpler `QUICKLYA` treatment have the same box size of $80h^{-1}$ comoving Mpc and have 2×512^3 or 2×1024^3 particles, respectively.

The cosmological parameters for all the simulations are in agreement with either Hinshaw et al. (2013) or Planck Collaboration et al. (2014). Simulated spectra are extracted from all models at $z = 0.1$ along 1000 random lines of sight (our results have converged for this number of spectra). Resolution effects are taken into account by convolution with the COS LSF. The S/N per resolution element is chosen to be 30. The simulated spectra are then analysed with `VPFIT` adapted for de-convolution of the COS LSF, using the same procedure used to fit the observational data. Although we will show data for a wider range of column densities, it is only the range between $N_{\rm H\,I} = 10^{13-14}$ cm^{-2} that we found to be robust with regard to resolution and noise issues (we discuss this further below). Unless otherwise stated, we therefore scale the mean transmitted flux of the spectra to match the observed column density distribution function (CDDF) in this range. This rescaling is performed by modifying the optical depth in each pixel of the simulated spectra by a constant, $A_{\rm f}$, such that $\overline{F}_{\rm f} = \langle e^{-A_{\rm f}\tau_{\rm i}} \rangle$. Table 1 summarises the simulations along with some quantities discussed in the following sections.

We have also performed a series of convergence checks on the simulations. With regard to mass resolution, when

Model	Γ	T_0	T_+	$\overline{F}$	A_f	$\overline{F}_\mathrm{f}$	Γ_f
HM01	0.127	3.72	4.93	0.985	1.252	0.982	0.101
$HM01_{hot}$	0.127	3.99	5.00	0.989	2.007	0.981	0.063
$HM01_{vhot}$	0.127	4.08	5.00	0.990	2.426	0.980	0.052
HM12	0.035	3.71	4.90	0.964	0.408	0.981	0.087
$HM12_{hot}$	0.035	3.97	4.94	0.972	0.624	0.981	0.057
Illustris	0.048	3.73	6.19	0.976	0.982	0.977	0.049
Sherwood	0.035	3.91	5.12	0.965	0.496	0.979	0.071

Table 1. Hydrodynamical simulations used in this work. The columns list: the simulation name; the H I photoionisation rate, Γ, in units of $10^{-12}\,\mathrm{s}^{-1}$; T_0, the median temperature at the mean density (log. units, volume weighted) calculated for a random sampling of gas at $\log(1+\delta) = [-0.1,0.1]$ and excluding gas hotter than 10^5 K; T_+, the median temperature for overdensities $\delta = [4-40]$ (log. units); the simulated mean transmitted flux; the rescaling factor A_f applied to match the CDDF in the range $\log(N_\mathrm{HI}/\mathrm{cm}^{-2})$ =[13-14]; the mean flux obtained; the new $\Gamma_\mathrm{f} = \Gamma/A_\mathrm{f}$ value inferred from the rescaling. Quantities are at $z = 0.1$.

comparing the CDDFs of the `QUICKLYA` Sherwood runs (not shown in Table 1) we found agreement at the 15 per cent level in the range $\log(N_\mathrm{HI}/\mathrm{cm}^{-2}) = 12.5 - 14.5$ while the b-parameter distributions agree to within 20 per cent at $> 20\,\mathrm{km\,s}^{-1}$. Regarding box size effects, we found that the HM12, Sherwood and Illustris simulations are all in very good agreement; box sizes of $60h^{-1}$ comoving Mpc are large enough to effectively probe the range of column densities considered here. The same holds for the b-parameter distribution. In terms of the sub-grid physics, when we compare a simulation with the effective star formation model of Springel & Hernquist (2003) (not shown in the table) with the `QUICKLYA` HM runs we find that the CDDF and b-parameter distributions are in good agreement: the CDDFs agree within 10 per cent in the range $\log(N_\mathrm{H\,I}/\mathrm{cm}^{-2}) = 12.5 - 14.5$, while the b-parameter distribution agrees within 25 per cent over the whole range. Since these errors are smaller than the statistical uncertainties of the data, for our purposes `QUICKLYA` does not significantly impact on the column density range considered here when compared to a more detailed star formation model. Finally, the $b-$parameter distribution from Illustris is converged within 10 per cent when using S/N values in the range 20-40 per resolution element (the reference case is 30) at 17-70 $\mathrm{km\,s}^{-1}$, while the CDDFs agree within 0.05 dex in the range $\log(N_\mathrm{H\,I}/\mathrm{cm}^{-2}) = 13 - 14.5$.

4 RESULTS

In Fig. 1 (left) we show the main result of the present work: the line width distributions for the simulations and COS data. It is clear that HM01 and Illustris do not provide a good fit to the data. The most problematic ranges are at $b = 25 - 45\ \mathrm{km\,s}^{-1}$, where HM01 and Illustris underpredict the number of lines by roughly a factor of two, and below 20 $\mathrm{km\,s}^{-1}$ where these models are a factor of four higher than the data. The Sherwood simulation is in better agreement with the data, although it still slightly overpredicts (underpredicts) the number of lines at $< 20\mathrm{km\,s}^{-1}$ ($b = 40$–$60\,\mathrm{km\,s}^{-1}$). We should caution here, however, that the distribution at $b < 20\ \mathrm{km\,s}^{-1}$ is not fully converged with mass resolution for the HM and Sherwood simulations, and will slightly underpredict the incidence of narrow lines. However, this regime is numerically converged for Illustris. The median $b-$values are 28.0, 34.5, 36.5 $\mathrm{km\,s}^{-1}$ for HM01, $\mathrm{HM01_{hot}}$, $\mathrm{HM01_{vhot}}$, respectively; 32.9 $\mathrm{km\,s}^{-1}$ for $\mathrm{HM12_{hot}}$ and 28.3 and 33.6 $\mathrm{km\,s}^{-1}$ for Illustris and Sherwood, respectively, while the COS data have a median of 36.2 $\mathrm{km\,s}^{-1}$.

Only the $\mathrm{HM01_{hot}}$ and $\mathrm{HM12_{hot}}$ simulations, which have been obtained by multiplying the He II photo-heating rates by a factor of three, are in good agreement with the data. Here $\mathrm{HM01_{hot}}$ is around 17 000 K (4000 K) hotter than HM01 at $z = 0.1$ for overdensities $\delta = 4 - 40$ ($\delta = 0$). For the corresponding HM12 simulation the change in temperature is similar. $\mathrm{HM01_{vhot}}$, in which the He II photo-heating rate has been increased by a factor of five, is instead too hot and underpredicts the number of narrow lines with $b < 25\,\mathrm{km\,s}^{-1}$.

Interestingly, the Illustris simulation is remarkably close to the HM01 model, despite the considerable differences in the sub-grid physics used in these simulations. In the right panel of Fig. 1 we show the probability distribution function (PDF) of the gas temperature for overdensities $\delta = 4 - 40$ – this selects systems in the column density range considered in this work (cf. Schaye 2001). The HM01 model is too cold to produce broad lines; the $\mathrm{HM01_{vhot}}$ model instead has a PDF peaking at $10^{4.35}$ K and in general more gas in the range $10^{4.25-5}$ K due to enhanced photo-heating. The Sherwood run has temperatures closer to that of $\mathrm{HM01_{vhot}}$ and $\mathrm{HM01_{hot}}$ runs, although also exhibits a peak at 10^5 K arising from galactic feedback. In contrast, the Illustris simulation shows much higher temperatures, with a PDF that peaks at $10^{6.5}$ K; this hot gas is too collisionally ionised to produce Ly-α absorption, resulting in a similar b-parameter distribution to HM01. This is due to the very energetic AGN bubble injections in Illustris which drive strong shocks that travel into the IGM and fill most of the volume at $z \sim 0.1$.

Finally, we have also analysed further simulations not presented in Fig. 1 with a wider range of feedback implementations. A Sherwood run with only stellar feedback results in an increase by roughly $3\mathrm{km\,s}^{-1}$ in the peak of the $b-$parameter distribution with respect to a `QUICKLYA` model, while the implementation of AGN feedback (orange solid line in Fig. 1) increases this value further by another $2\,\mathrm{km\,s}^{-1}$. Similarly, an increase of $4\mathrm{km\,s}^{-1}$ in the peak of the distribution was found when comparing a kinetic wind implementation with $480\mathrm{km\,s}^{-1}$ winds with the HM01 run. This demonstrates the impact of stellar and AGN feedback on the IGM temperature distribution is strong, and suggests the Ly-α forest b-parameter distribution is a useful diagnostic of galactic feedback in the low redshift Universe.

In the left panel of Fig. 2 we also compare the CDDF, $f = d^2N/d\log N_\mathrm{HI}dz$, of the simulations to the COS data. The HM01 and the Illustris simulations – the latter uses the Faucher-Giguère et al. (2009) UVB model – are in good agreement with the data in the range $\log N_\mathrm{H\,I}/\mathrm{cm}^{-2}$=13-14, while the Sherwood and HM12 runs overpredict the number of absorption systems by a factor of ~ 2. The $\mathrm{HM12_{hot}}$ model results in better agreement (since the neutral hydrogen fraction scales approximately $T^{-0.7}$ through the recombination coefficient) but still lies significantly above the data. In this comparison, there is no rescaling of optical

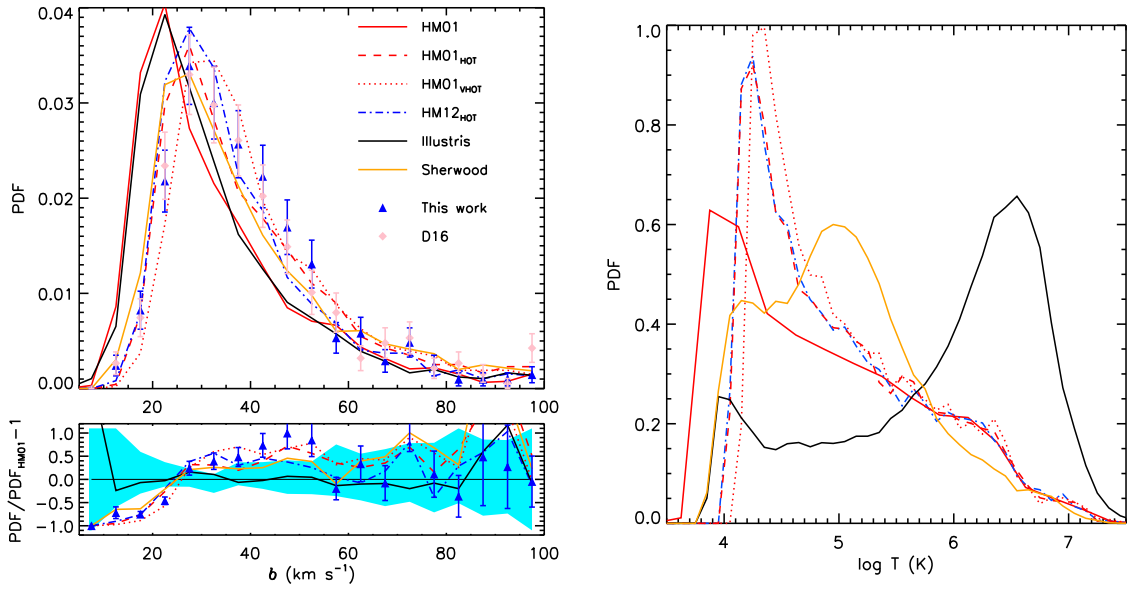

Figure 1. *Left.* The b-parameter distribution for HM01 (red solid line); $\mathrm{HM01_{hot}}$ (dashed red line); $\mathrm{HM01_{vhot}}$ (dotted red line); $\mathrm{HM12_{hot}}$ (blue dot-dashed line); Illustris (black solid line); Sherwood (orange solid line). The bottom panel shows the ratio of the line width PDFs with respect to HM01. The shaded area indicates the $\pm 2\sigma$ range obtained from a set of 100 mocks with the same redshift path as the data. COS data are represented by the blue triangles (Poisson error bars), while the D16 data are shown as pink diamonds. The spectra have been scaled to match the observed CDDF at $\mathrm{N_{HI}} = 10^{13-14}$ cm^{-2}, and only lines with $\mathrm{N_{HI}/cm^{-2}} = 10^{13-14}$ and for which the relative error on the b-parameter is smaller than 0.5 are used for all data shown. *Right.* Distribution of the volume weighted gas temperature when selecting gas with overdensities in the range $\delta = 4 - 40$.

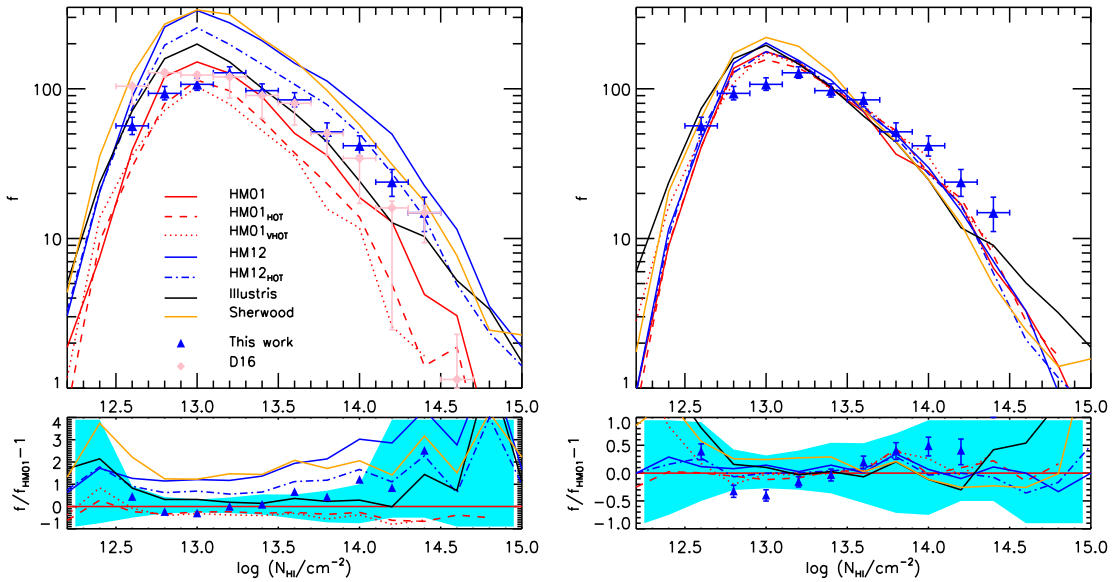

Figure 2. *Left.* The corresponding CDDF (log. scale) for the data described in Fig. 1 with the addition of the HM12 model (solid blue curve). No scaling has been applied to the mean transmission of the simulated spectra. *Right.* The effect of scaling the optical depths (and hence H I photo-ionisation rate) to fit the CDDF in the range $\log(N_{\mathrm{H\,I}}/\mathrm{cm}^{-2})$=13-14. Data are affected by incompleteness at $\log(N_{\mathrm{H\,I}}/\mathrm{cm}^{-2}) \leqslant 13$.

depths and these simulations have values of Γ and $\overline{F}$ as summarised in Table 1 (cf. $\overline{F} = 0.983$ from D16).

In the right panel we show what happens when we require the simulations to fit the CDDF in the range we consider most robust, $\log(N_{\mathrm{H\,I}}/\mathrm{cm}^{-2}) = 13{-}14$, by rescaling the optical depths in the mock spectra. The values of the mean transmitted flux, $\overline{F}_{\mathrm{f}}$, and photo-ionisation rate, Γ_{f} inferred are listed in Table 1. Overall, we find that the mean transmitted fluxes are in the range $\overline{F}_{\mathrm{f}} = [0.977 - 0.982]$, in good agreement with the D16 value (we have verified that matching the D16 mean transmitted flux or the CDDF at these column densities is roughly equivalent), and the inferred photo-ionisation rates are in the range $\Gamma_{\mathrm{f}} = [0.05{-}0.1] \times 10^{-12}$ s^{-1}. The latter are a factor 1.5–3 higher than predicted by the widely used HM12 UVB model and are in very good agreement with the recent results of Shull et al. (2015). Note also

the effects of feedback appear to be more prominent for absorbers with column densities $\log(N_{\rm H\,I}/{\rm cm}^{-2}) > 14.5$.

5 CONCLUSIONS

We have used hydrodynamic simulations to explore several properties of the Ly-α forest at $z = 0.1$: the b-parameter distribution, CDDF and mean transmitted flux. The simulations probe a wide range of different UVBs, feedback and star formation implementations, box sizes and resolutions. We find that several simulations fail in reproducing the line width distribution, under-predicting the number of lines with b-parameter values 25-45 km s^{-1} by a factor of two when compared to the observational data. This is either because the gas is too cold or, in models with vigourous AGN feedback, collisionally ionised. This tension is partly alleviated when considering alternative feedback models (less aggressive AGN feedback and galactic winds) used in the Sherwood run but it only disappears in an *ad-hoc* model with enhanced photo-heating, resulting in a median temperature 10^5 K for the IGM with overdensities $\delta = [4 - 40]$.

The CDDF and mean flux are furthermore reproduced only if the photo-ionisation rate is higher than predicted by the HM12 model by at least a factor 1.5. The discrepancy between the values of the photo-ionisation rate required to match the COS data with those predicted by the HM12 model is around a factor of 2, rather than the factor 5 suggested by (Kollmeier et al. 2014). This is largely due to the presence of hot(ter) gas in our simulations. Overall, we conclude that comparison of models to the observed b-parameter distributions provides a valuable diagnostic of feedback in the low redshift IGM, and may help pinpoint any missing physical ingredients in current hydrodynamic simulations in the form of additional or different thermal feedback or turbulence (e.g Iapichino et al. 2013).

ACKNOWLEDGMENTS.

MV is supported by INFN/PD51 Indark, and (with TSK) ERC Grant 257670-cosmoIGM. JSB is supported by a Royal Society URF. MGH and EP acknowledge support from the FP7 ERC Grant Emergence-320596 and the Kavli Foundation. Simulations were performed at the University of Cambridge with Darwin-HPCS and COSMOS, operated on behalf of the STFC DiRAC facility (funded by BIS National E-infrastructure capital grant ST/J005673/1 and STFC grants ST/H008586/1, ST/K00333X/1), and on the Curie supercomputer at TGCC through the 8th PRACE call. BPW is supported by NASA grants HST-AR-12842, HST-AR-13893 from STSCI operated by AURA under contract NAS5-26555 and AST-1108913 by NSF.

REFERENCES

Bolton J. S., Puchwein E., Sijacki D., Haehnelt M. G., Kim T.-S., Meiksin A., Regan J. A., Viel M., 2016, MNRAS in press, arXiv:1605.03462
Bolton J. S., Viel M., Kim T.-S., Haehnelt M. G., Carswell R. F., 2008, MNRAS, 386, 1131
Carswell R. F., Webb J. K., 2014, VPFIT, Astrophysics Source Code Library, record ascl:1408.015
Danforth C. W. et al., 2016, ApJ, 817, 111
Davé R., Oppenheimer B. D., Katz N., Kollmeier J. A., Weinberg D. H., 2010, MNRAS, 408, 2051
Faucher-Giguère C.-A., Lidz A., Zaldarriaga M., Hernquist L., 2009, ApJ, 703, 1416
Ford A. B., Oppenheimer B. D., Davé R., Katz N., Kollmeier J. A., Weinberg D. H., 2013, MNRAS, 432, 89
Gurvich A., Burkhart B., Bird S., 2016, preprint, arXiv:1608.03293
Haardt F., Madau P., 2001, in Clusters of Galaxies and the High Redshift Universe Observed in X-rays, Neumann, D. M. & Tran, J. T. V. ed., astro-ph/0106018 Modelling the UV/X-ray cosmic background with CUBA
Haardt F., Madau P., 2012, ApJ, 746, 125
Hinshaw G. et al., 2013, ApJS, 208, 19
Iapichino L., Viel M., Borgani S., 2013, MNRAS, 432, 2529
Janknecht E., Reimers D., Lopez S., Tytler D., 2006, A&A, 458, 427
Khaire V., Srianand R., 2015, MNRAS, 451, L30
Kim T.-S., Carswell R. F., Mongardi C., Partl A. M., Mücket J. P., Barai P., Cristiani S., 2016, MNRAS, 457, 2005
Kim T.-S., Partl A. M., Carswell R. F., Müller V., 2013, A&A, 552, A77
Kirkman D., Tytler D., Lubin D., Charlton J., 2007, MNRAS, 376, 1227
Kollmeier J. A. et al., 2014, ApJ, 789, L32
Kriss G. A., 2011, COS Instrument Science Report 2011-01(v1), 17 pages, p. 1
Pachat S., Narayanan A., Muzahid S., Khaire V., Srianand R., Wakker B. P., Savage B. D., 2016, MNRAS, 458, 733
Planck Collaboration et al., 2014, A&A, 571, A16
Puchwein E., Springel V., 2013, MNRAS, 428, 2966
Rahmati A., Schaye J., Crain R. A., Oppenheimer B. D., Schaller M., Theuns T., 2016, MNRAS, 459, 310
Savage B. D., Kim T.-S., Wakker B. P., Keeney B., Shull J. M., Stocke J. T., Green J. C., 2014, ApJS, 212, 8
Schaye J., 2001, ApJ, 559, 507
Shull J. M., Danforth C. W., Tilton E. M., 2014, ApJ, 796, 49
Shull J. M., Moloney J., Danforth C. W., Tilton E. M., 2015, ApJ, 811, 3
Sijacki D., Springel V., Di Matteo T., Hernquist L., 2007, MNRAS, 380, 877
Springel V., 2005, MNRAS, 364, 1105
Springel V., 2010, MNRAS, 401, 791
Springel V., Hernquist L., 2003, MNRAS, 339, 289
Tornatore L., Borgani S., Viel M., Springel V., 2010, MNRAS, 402, 1911
Viel M., Haehnelt M. G., Springel V., 2004, MNRAS, 354, 684
Villaescusa-Navarro F. et al., 2016, MNRAS, 456, 3553
Vogelsberger M., Genel S., Sijacki D., Torrey P., Springel V., Hernquist L., 2013, MNRAS, 436, 3031
Vogelsberger M. et al., 2014, Nat, 509, 177
Wakker B. P., Hernandez A. K., French D. M., Kim T.-S., Oppenheimer B. D., Savage B. D., 2015, ApJ, 814, 40
Werk J. K. et al., 2016, ApJ submitted, arXiv:1609.00012
Weymann R. J. et al., 1998, ApJ, 506, 1